Journal of Ultrafine Grained and Nanostructured Materials
https://jufgnsm.ut.ac.ir
Vol. 50, No.2, December 2017, pp. 152-160
Print ISSN: 2423-6845 Online ISSN: 2423-6837
DOI: 10.22059/JUFGNSM.2017.02.10

Analysis of Strengthening Mechanisms in an Artificially Aged Ultrafine Grain 6061 Aluminum Alloy

Mohammad Reza Rezaei*[*,1], Mohammad Reza Toroghinejad[2], Fakhreddin Ashrafizadeh[2]

[1]School of Engineering, Damghan University, Damghan, Iran.
[2]Department of Materials Engineering, Isfahan University of Technology, Isfahan, Iran.

Recieved: 17 September 2017; Accepted: 4 December 2017
** Corresponding author email: m.r.rezaei@du.ac.ir*

ABSTRACT
The current study adopted a quantitative approach to investigating the mechanical properties, and their relationship to the microstructural features, of precipitation-strengthened 6061 aluminum alloy processed through accumulative roll bonding (ARB) and aging heat treatment. To serve this purpose, the contributions of different strengthening mechanisms including grain refinement, precipitation, dislocation and solid-solution strengthening to the yield strength of five-cycle ARB samples processed under pre-aged (ARBed) and aged (ARBed+Aged) conditions were examined and compared. Microstructural characterizations were performed on the samples through the transmission electron microscope (TEM) and X-ray diffraction (XRD). Also, the mechanical properties of the samples were investigated through the tensile test. The obtained results showed that an equiaxed ultrafine grain structure with nano-sized precipitates was created in the both ARBed and ARBed+Aged samples. The grain refinement was the predominant strengthening mechanism which was estimated to contribute 151 and 226 MPa to the ARBed and ARBed+Aged samples, respectively, while the dislocation and Orowan strengthening mechanisms were ranked second with regard to their contributions to the ARBed and ARBed+Aged samples, respectively. The overall yield strength, calculated through the root mean square summation method, was found to be in good agreement with the experimentally determined yield strength. It was also found that the presence of non-shearable precipitates, which interfered with the movement of the dislocations, would be effective for the simultaneous improvement of the strength and ductility of the ARBed+Agedsample .

Keywords: *Accumulative roll bonding (ARB); Aging; Strengthening mechanisms; Microstructure; Mechanical properties.*

How to cite this article:
Rezaei MR, Toroghinejad MR, Ashrafizadeh F. Analysis of Strengthening Mechanisms in an Artificially Aged Ultrafine Grain 6061 Aluminum Alloy . J Ultrafine Grained Nanostruct Mater, 2017; 50(2):152-160.

1. Introduction

Different strengthening mechanisms such as grain-boundary strengthening (Hall–Petch effect), work hardening, solid-solution strengthening, and precipitation strengthening are responsible for the relatively high strength of metals and alloys [1-3]. All of these mechanisms are concerned with some microstructural features of materials. It is well-known that some processes (e.g., plastic deformation and heat treatment) alter the microstructural characteristics of materials, which, in return, affects their related strengthening mechanisms and mechanical properties. For example, severe plastic deformation (SPD) processes have been used for grain refinement to a submicron scale and enhancement of the mechanical properties of different metals and alloys [4-7]. These refined materials have proved to

be suitable candidates for engineering applications such as structural materials and high-performance and reliable parts in automobile, aircraft, and electronic industries [8,9]. One of the most important SPD techniques is accumulative roll bonding (ARB) which can be applied to several cycles of the production process in order to obtain homogenous ultrafine grain structures in metallic materials [10]. Some studies have combined the aging heat treating processes, which are affective for improving the mechanical properties of heat treatable alloys, with the ARB processes in order to acquire more preferable mechanical properties [11,12]. Metastable structures developed through the ARB processes can modify the precipitation of the second phases in the microstructure of heat treatable alloys with the help of the aging processes [11]. For example, it has been shown that the size and morphology of precipitates are influenced by high-dislocation density regions created during the ARB processes [13]. However, in the literature, the effects of the microstructural features of materials on the mechanical properties of severely deformed and aged samples have been discussed only qualitatively [14,15].

The AA6061 aluminum alloy is one of the Al Mg Si (Cu) system alloys which can be significantly strengthened via proper aging heat treatments. This alloy is known for its medium strength and excellent formability [16,17]. Thus, it is usually considered as a suitable candidate for studying the effects of combining ARB, as a forming process, and aging heat treatment on the mechanical properties of materials.

To the knowledge of the researchers, no attempt has been undertaken till now to quantify the strengthening mechanisms in the ARBed+Aged alloys to be able to estimate the contributions of relevant strengthening mechanisms and then, provide reasonable models for prediction and comparison of their strengths. It is argued that quantitative approaches help design accurate models of materials and processes which, in return, help achieve desirable mechanical properties.

Hence, the aim of this study is to quantify the contributions of all the effective strengthening mechanisms and calculate the overall strengths of the ARBed and ARBed+Aged 6061 aluminum alloys by means of precise microstructural surveys and related mathematical equations.

2. Experimental procedures

2.1. ARB and Aging processes

The material initially used in this study was the 6061 aluminum alloy which had been fully annealed at 803K for 1.5 h. The strips of thematerial were cut into 200mm×40mm×1mm pieces parallel to the sheet rolling direction. Then, the cycles of the ARB processing were consecutively performed on the strips which included degreasing, scratch brushing, and finally roll bonding . The last cycle was carried out by using a labratoary roll mill with the reduction equal to 50% (load capacity and rolling speed were 20 tones and 2 m/min, respectively) . Once each cycle was performed, the roll-bonded strips were cut in half; the procedure was repeated five times at an ambient temperature. Then, the aging processing was performed on the five cyles of the ARBed samples at 373 K for 48 hours, resulting in the ARBed+Aged samples. As mentioned earlier, this was the optimal heat treatment regime which would enhance both the strength and ductility of the ARBed sample [13].

2.2. Microstructure evaluation and mechanical properties

The microstructre of the samples targeted in this study was examined on the RD-TD plane of the thin foil samples, preparad through twin jet electropolishing in a A2 Struers solution, by using a Philips CM12 transmission electron microscope (TEM) operating at 120 kV and the microstructural features were quantified by using a Clemex Vision image analyzer. X-ray diffraction analysis was then carried out to calculate the dislocation density of the samples. The XRD pattern of the consolidated composite between 20° and 90°was examined by using a Philips X'PERT MPD diffractometer with Cu Kα radiation. The following equations were used to estimate the stored dislocation density (ρ) in the samples [18]:

$$\rho = (\rho_D \times \rho_s)^{1/2} \quad \text{(eq. 1)}$$

$$\rho_D = \frac{3}{D^2} \quad \text{(eq. 2)}$$

$$\rho_s = \frac{6\pi\varepsilon^2}{b^2} \quad \text{(eq. 3)}$$

Where D and ε are the average values of the crystallite size and lattice microstrain, respectively, and b is the Burgers vector. The Williamson-Hall

equation was used to calculate the crystallite size and lattice microstrain as follows [19]:

$$\beta \cos\theta = \frac{K\lambda}{D} + 4\varepsilon \sin\theta \qquad \text{(eq. 4)}$$

Where β represents the full widths at the half maximum (FWHM) of a diffraction peak, θ is the diffraction angle, λ is the wave length of X-rays and k is a constant. The Williamson–Hall method requires that two variables equation system be solved and it needs at least two diffraction peak angles. Here, β *cos*θ is plotted versus *sin*θ by considerng four intensity peaks belonging to the (111), (200), (220), and (311) crystallographic planes where the intercept and slope of the trend line present the crystallite size and lattice microstrain, respectively.

Following the ASTM E8M standard, the mechanical properties of the samples were examined through the standard tensile test by using a Houndsfield H50KS testing machine running at a strain rate of 1.67×10^{-4} s^{-1}. The samples in the tensile test were oriented along the rolling direction while the gauge length and width of the samples were respectively 25 and 6 mm. The tensile test was repeated 3 times for each of the samples.

3. Results

3.1. Microstructure observation

TEM microstructures and the corresponding selected area diffraction patterns (SAD) of the ARBed and ARBed+Aged samples are illustrated in Fig. 1. Fig. 1(a) shows that the ARBed sample consisted of submicron grains with an average size of 240 nm and that almost all the grains were separated by clear-cut grain boundaries. According Fig. 1(a), some of the grey precipitates with a volume fraction of 0.01 and an average diameter of 71 nm were created in the microstructures.

Fig. 1(b) shows that, once the aging processing was performed, the average grain size of the ARBed+Aged sample changed (i.e., it reached 280 nm) and its microstructure was filled with some white and grey precipitates with a spherical

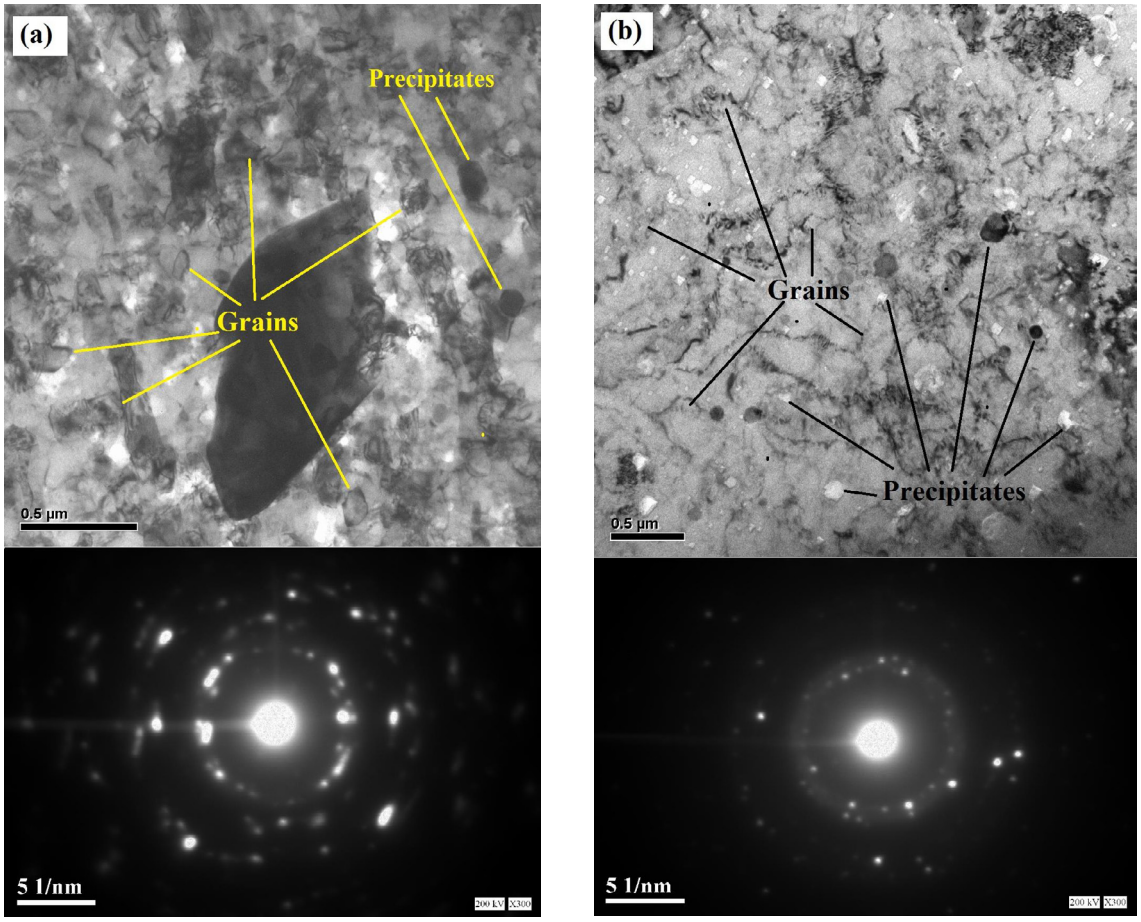

Fig. 1- TEM micrographs and the matching SAD patterns of (a) the ARBed and (b) ARBed+Aged samples.

morphology. Following the ASTM E 1245 standard that the volume fraction of each phase of a microstructure would be equivalent to its area fraction, the volume fraction and mean diameter of the precipitates were respectively calculated to be 0.07 and 65 nm. These precipitates were created as a result of the depletion of alloying elements such as Mg and Si from the saturated solid solution. The SAD patterns of the both samples (Figs. 1 (a) and (b)) contain many spots situated around Debye–Scherrer circles that confirms the presence of a large number of grains separated with high angle boundaries in the selected area.

3.2. Dislocations density calculations

The X-ray diffraction patterns and Williamson-Hall plots of the ARBed and ARBed+Aged samples are presented in Fig 2. For both samples, only the diffraction peaks that belonged to Al appeared in the patterns. Because the diffracted waves would come from the phases with low quantity (almost lower than 10 vol% as was the case for the precipitates in the present study) they could not be detected through the XRD technique.

It is clear from Fig. 2 that some little changes in the peak intensity and width of the samples have occurred. Based on the Williamson-Hall equation, the stored dislocations density was calculated to be 3.32×10^{14} and 2.75×10^{14} m^{-2} for the ARBed and ARBed+Aged samples, respectively.

3.3. Mechanical properties

The engineering stress-strain curves belonging to the ARBed and ARBed+Aged samples are shown in Fig. 3. Table 1 represents the mechanical properties obtained from these curves. The results obtained showed that the yield and tensile strength of the ARBed sample respectively increased to 101 and 92 MPa after aging process was performed. Also, the elongation of the ARBed+Aged sample was 2.5% higher compared to that of the ARBed sample. It should be emphasized that, as shown in Table 2, the improvement in the ductility of the samples can be largely attributed to the increase in the uniform elongations.

4. Discussion

The mechanical properties of the ARBed and ARBed+aged samples can be related to their microstructural features and these properties can be quantified through corresponding strengthening mechanisms. The contributions of various strengthening mechanisms to the total

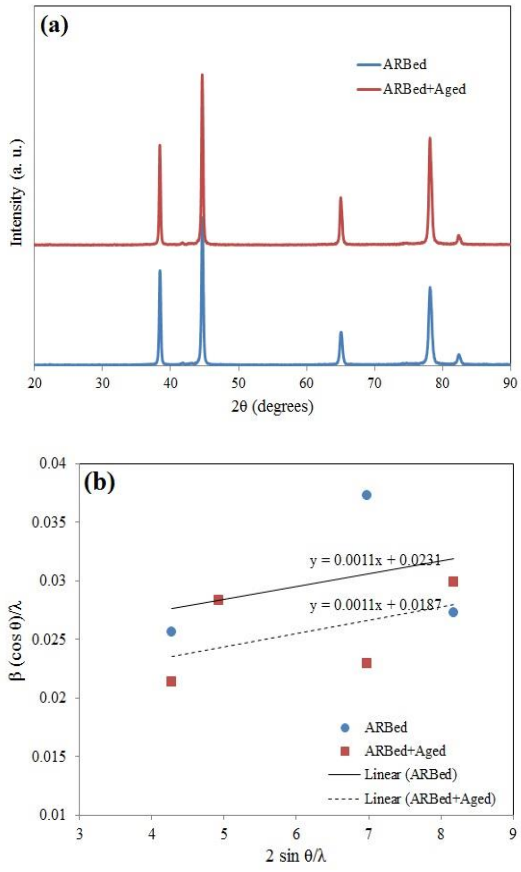

Fig. 2- (a) The XRD patterns and (b) Williamson–Hall plots of the ARBed and ARBed+Aged samples.

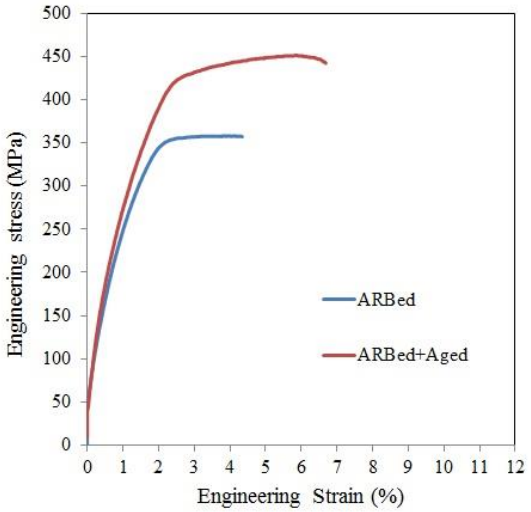

Fig. 3- The engineering stress-strain curves of the ARBed and ARBed+Aged samples.

yield strength of the both samples are discussed below.

4.1. Solid-solution (solute) strengthening

This strengthening mechanism occurs due to the Cottrell atmosphere of solute elements around lattice dislocations that impede the movement of dislocations [20]. In other words, solute atoms that differ from matrix atoms in size and/or shear modulus cause variations in the strain fields around dislocations. In the field of materials engineering, the Fleischer equation is accepted to provide a good estimate of solid-solution strengthening mechanism even in ultrafine grain structures [21,22]:

$$\Delta\sigma_{ss} = MGb\varepsilon_{ss}^{3/2}\sqrt{c} \quad \text{(eq. 5)}$$

$$\varepsilon_{ss} = |\acute{\varepsilon}_G - \beta\varepsilon_b| \quad \text{(eq. 6)}$$

$$\acute{\varepsilon}_G = \frac{\varepsilon_G}{1+\frac{1}{2}|\varepsilon_G|} \quad \text{(eq. 7)}$$

$$\varepsilon_G = \frac{1}{G}\frac{dG}{Dc} \quad \text{(eq. 8)}$$

$$\varepsilon_b = \frac{1}{a}\frac{da}{dc} \quad \text{(eq. 9)}$$

Where M is the Taylor factor (equal to 3.06 for polycrystalline fcc materials such as aluminum [23]), G is the shear modulus (~25.4 GPa for aluminum [24]), b is the Burgers factor vector (equal to 0.286 nm [25]), ε_{ss} is the lattice strain, c is the atomic concentration of a solute, β is a constant equal to 3, and α is the lattice parameter of the matrix. It is assumed that solute atoms entirely deplete from solid solutions under aged conditions and hence, this strengthening mechanism was only deployed to the ARBed sample. Mg and Si are the most effective solute atoms in the solid solution strengthening of the 6061 aluminum alloy. By substituting values for the parameters in the above equations, the increase in the strength resulting from Mg and Si was calculated to be 35.92 and 0.52 MPa, respectively. Thus, the solute strengthening contributed a total increase of 36.45 MPa for the ARBed sample.

4.2. Orowan strengthening (Precipitation Strengthening)

This strengthening mechanism originates from the interaction between nano-sized precipitates and lattice dislocations. Hence, the Orowan strengthening mechanism mainly works with aged samples. The strengthening through this mechanism can be quantified through the following equation [2]:

$$\Delta\sigma_{Oro} = \frac{0.8MGb}{2\pi\lambda(1-\upsilon)^{1/2}}\ln\left(\frac{x}{2b}\right) \quad \text{(eq. 10)}$$

Table 1- The tensile mechanical properties of the ARBed and ARBed+Aged samples

	Yield strength (MPa)	Tensile strength (MPa)	Uniform elongation (%)	Total elongation (%)
ARBed	299	357	3.9	4.2
ARBed+Aged	400	449	5.7	6.7

Table 2- Estimated contributions of the strengthening mechanisms to the samples

	ARBed	ARBed+Aged
Solid solution, $\Delta\sigma_{ss}$ (MPa)	36.45	-
Precipitates, $\Delta\sigma_{Oro}$ (MPa)	38.45	126.22
Grain refinement, $\Delta\sigma_{H-P}$ (MPa)	151.05	226.78
Dislocations, $\Delta\sigma_{Dis}$ (MPa)	97.21	88.47

Where υ is the Poisson's ratio that is about 0.33, λ is the interparticle distance, and is the mean diameter of the precipitates on the slip plane. The parameters λ and x can be calculated through the following equations:

$$\lambda = \sqrt{\frac{2}{3}}\left(\sqrt{\frac{\pi}{4f}} - 1\right)d_P \qquad \text{(eq. 11)}$$

$$x = \sqrt{\frac{2}{3}}d_P \qquad \text{(eq. 12)}$$

Where f is the volume fraction and d_p is the mean diameter of the precipitates already determined by the TEM observation (see section 3.1). In this study, $\Delta\sigma_{Orowan}$ was calculated to be 38.45 and 126.22 MPa for the ARBed and ARBed+Aged samples, respectively.

4.3. Grain refinement strengthening

This is another important strengthening mechanism that is caused by the change in the direction of moving dislocations when the dislocations pass from one grain to neighboring grains along grain boundary regions which restrict their movements. The process of grain refinement up to the ultrafine level would lead to the higher density of the grain boundaries, resulting in the strengthening of the material. This phenomenon is described by the Hall-Petch equation shown to be valid in the case ultrafine grain sizes [26]:

$$\Delta\sigma_{H-P} = kd^{-1/2} \qquad \text{(eq. 13)}$$

Where k is the Hall-Petch slope that is ~ 74 and 120 $MP_a(\mu m)^{-1/2}$ for the age hardenable aluminum alloy in solid solutions and under aged conditions, respectively [25] and d is the average grain size determined in section 3.1. After substituting values for the parameters in the equation, the increase in the strength resulting from the grain refining mechanism was calculated to be 81.65 and 75.59 MPa for the ARBed and ARBed+Aged samples, respectively.

4.4. Work hardening or dislocation strengthening

The Strengthening through this mechanism arises from the interaction between the strain fields around moving dislocations that hinder their movement, resulting in the strengthening of the material. Increase in the strength of the material through the dislocation strengthening mechanism can be calculated through the Bailey–Hirsch equation as follows [27]:

$$\Delta\sigma_{Dis} = M\alpha Gb\sqrt{\rho} \qquad \text{(eq. 14)}$$

Where α is a constant equal to 0.24 and ρ is the dislocation density stored in the lattice as calculated in section 3.2. In this study, the contribution of the dislocation strengthening to the ARBed and

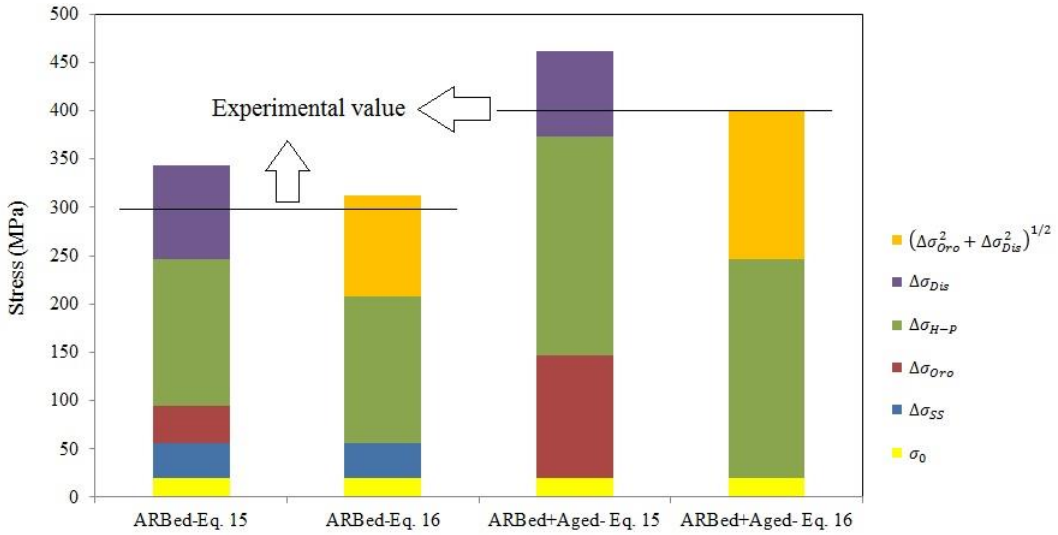

Fig. 4- Comparison of the experimental and theoretical strengths for the ARBed and ARBed+Aged samples.

ARBed+Aged samples was calculated to be 97.21 and 88.47 MPa, respectively.

Table 2 summarizes the contribution of each of the strengthening mechanisms examined in this study to the both ARBed and ARBed+Aged samples. According to the table, grain refinement is the most effective strengthening mechanism for increasing the strength of ARBed and ARBed+Aged samples. On the other hand, the second effective strengthening mechanisms for ARBed and ARBed+Aged samples are respectively dislocation strengthening and precipitation strengthening . Hence, it can be concluded the ultrafine grains created through the process of continuous recrystallization highly interfere with the motion of dislocations, which results in significant increase in the yield strength of ARBed samples. The process of continuous recrystallization accompanied by the annihilation of the stored dislocations caused the role of the strain hardening to decrease during the process of strengthening the ARBed sample. Although some grain growth occurred after the aging process, the process of the grain refinement still made the most contribution to the increase in the strength of the ARBed+Aged sample. It should be mentioned that, in addition to the constructive role of the nano-sized precipitates in the Orowan strengthening mechanism, these precipitates have the ability to pin the grain boundaries during the aging process [28]. Thus, non-shearable precipitates would indirectly influence the grain refinement strengthening mechanism and exert a dual effect on the strength of the ARBed+Aged sample. According to the previous research [25], for an ultrafine grain 7075 aluminum alloy (produced through consolidating the nanocrystalline powder) which subsequently aged at 393 K for 24 h, Orowan mechanism was determined as the most effective strengthening mechanism. In the above-mentioned research, the grain size and mean diameter of precipitates was about 422 nm and 4 nm, respectively. Thus, based on Eq. 10 and 13, the Orowan strengthening mechanism could play a more effective role (compared to grain refinement) in strengthening of the 7075 aluminum alloy.

The overall yield strength of the ARBed and ARBed+Aged samples can be calculated through linear addition of the contributions of the effective mechanisms as follows [29,30]:

$$\sigma_y = \sigma_0 + \Delta\sigma_{ss} + \Delta\sigma_{Oro} + \Delta\sigma_{H-P} + \Delta\sigma_{Dis} \qquad \text{(eq. 15)}$$

Where σ_0 is the friction stress that is about 20 MPa for aluminum [23]. The values of the experimental and theoretical strengths (calculated through Eq. 15) are compared in Fig 4 in which a significant difference of about 13 % can be observed between the theoretical and experimental yield strengths for both the ARBed and ARBed+Aged samples.

It is argued that it is not appropriate to add

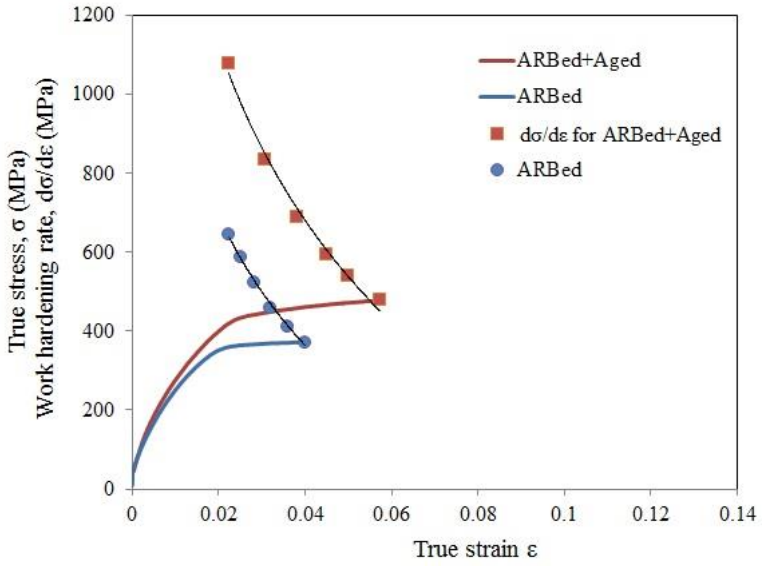

Fig. 5- True stress/true strain and strain hardening rate/true strain curves of the ARBed and ARBed+Aged samples.

strengthening contributions of dislocations and precipitates in a linear fashion, especially when the spacing of dislocations and precipitates is very small [2]. If the average spacing of dislocations is considered equal to $\rho^{-1/2}$, then, based on the dislocation densities calculated, the average spacing of a dislocation for the ARBed and ARBed+Aged samples would be ~ 55 and ~ 60 nm, respectively. Also, based on Eq. 11, the average spacing between the precipitates was calculated to be ~ 124 nm for the ARBed+Aged sample. In this situation, the strengthening performed through the precipitation and dislocation mechanisms was calculated via the root mean square summation, instead of linear addition. Alternatively, the following model can be used to predict the strength of the material [2]:

$$\sigma_y = \sigma_0 + \Delta\sigma_{ss} + \Delta\sigma_{H-P} + \sqrt{\Delta\sigma_{Oro}{}^2 + \Delta\sigma_{Dis}{}^2} \qquad \text{(eq. 16)}$$

The values of the yield strength for the ARBed and ARBed+Aged samples, calculated through Eq. 16, are also illustrated in Fig. 4. The figure shows that the yield strength is in reasonable agreement with the experimental values for both the ARBed and ARBed+Aged samples. Thus, it can be concluded that Eq. 16 estimates the yield strength of the ARBed and ARBed+Aged samples much better than Eq. 15.

The simultaneous increase in the strength and ductility of the ARBed+Aged sample with respect to the ARBed sample can be calculated through the following relation [31]:

$$\sigma \geq \left(\frac{d\sigma}{d\varepsilon}\right) \qquad \text{(eq. 17)}$$

Where σ and ε are the true stress and true strain, respectively, and $(\frac{d\sigma}{d\varepsilon})$ is the strain hardening rate. The true stress/true strain curves and the strain hardening rate/true strain curves for the ARBed and ARBed+Aged samples are illustrated in Fig. 5. The plastic instability (i.e., macroscopic necking) occurs at the meeting point of the two curves before which the elongation is uniform.

In Fig. 5, the ARBed+Aged sample exhibits more strain hardening rate compared to the ARBed sample because the dislocation loops created around the non-shearable precipitates would put obstacles to the moving dislocations and consequently, improve the strain hardening capacity of the alloy. Therefore, the higher ductility of the ARB+Aged sample can be attributed to the positive influences of the fine precipitates on the strain hardening capacity which results in the higher uniform elongation of the material.

5. Conclusions

In this study, the mechanical properties of the 6061 aluminum alloy under ARBed and ARBed+Aged conditions with respect to different strengthening mechanisms were investigated. The main results and conclusions of the study are summarized as follows:

1. The predominant strengthening mechanism in this study for both the ARBed and ARBed+Aged samples was grain refinement.

2. The yield strength calculated via the root mean square summation method fits the experimental values reasonably well for the ARBed and ARBed+Aged samples.

3. The increase in the strength of the ARBed+Aged sample, compared to that of the ARBed sample, was coincident with the improvement of the ductility.

References:

1. Wen H, Topping TD, Isheim D, Seidman DN, Lavernia EJ. Strengthening mechanisms in a high-strength bulk nanostructured Cu–Zn–Al alloy processed via cryomilling and spark plasma sintering. Acta Materialia. 2013;61(8):2769-82.
2. Shen J, Li Y, Li F, Yang H, Zhao Z, Kano S, et al. Microstructural characterization and strengthening mechanisms of a 12Cr-ODS steel. Materials Science and Engineering: A. 2016;673:624-32.
3. Kamikawa N, Sato K, Miyamoto G, Murayama M, Sekido N, Tsuzaki K, et al. Stress–strain behavior of ferrite and bainite with nano-precipitation in low carbon steels. Acta Materialia. 2015;83:383-96.
4. Azushima A, Kopp R, Korhonen A, Yang DY, Micari F, Lahoti GD, et al. Severe plastic deformation (SPD) processes for metals. CIRP Annals. 2008;57(2):716-35.
5. Goto M, Kamil K, Han SZ, Euh K, Kim SS, Yokoho Y. Effects of grain refinement due to severe plastic deformation on the growth behavior of small cracks in copper. International Journal of Fatigue. 2013;50:63-71.
6. Faraji G, Yavari P, Aghdamifar S, Mashhadi MM. Mechanical and Microstructural Properties of Ultra-fine Grained AZ91 Magnesium Alloy Tubes Processed via Multi Pass Tubular Channel Angular Pressing (TCAP). Journal of Materials Science & Technology. 2014;30(2):134-8.
7. Riahi M, Ehsanian MH, Asgari A, Djavanroodi F. On a novel severe plastic deformation method: severe forward extrusion (SFE). The International Journal of Advanced Manufacturing Technology. 2017;93(1-4):1041-50.
8. Ortiz-Cuellar E, Hernandez-Rodriguez MAL, García-Sanchez E. Evaluation of the tribological properties of an Al–Mg–Si alloy processed by severe plastic deformation. Wear. 2011;271(9-10):1828-32.
9. Khatami R, Fattah-alhosseini A, Mazaheri Y, Keshavarz MK, Haghshenas M. Microstructural evolution and mechanical properties of ultrafine grained AA2024 processed by accumulative roll bonding. The International Journal of Advanced Manufacturing Technology. 2017;93(1-4):681-9.
10. Mohammad Nejad Fard N, Mirzadeh H, Mohammad

R, Cabrera J-M. Accumulative Roll Bonding of Aluminum/ Stainless Steel Sheets. Journal of Ultrafine Grained and Nanostructured Materials. 2017;50 (1):1-5
11. Tsuji N, Iwata T, Sato M, Fujimoto S, Minamino Y. Aging behavior of ultrafine grained Al–2 wt%Cu alloy severely deformed by accumulative roll bonding. Science and Technology of Advanced Materials. 2004;5(1-2):173-80.
12. Yu H, Su L, Lu C, Tieu K, Li H, Li J, et al. Enhanced mechanical properties of ARB-processed aluminum alloy 6061 sheets by subsequent asymmetric cryorolling and ageing. Materials Science and Engineering: A. 2016;674:256-61.
13. Rezaei MR, Toroghinejad MR, Ashrafizadeh F. Effects of ARB and ageing processes on mechanical properties and microstructure of 6061 aluminum alloy. Journal of Materials Processing Technology. 2011;211(6):1184-90.
14. Terada D, Kaneda Y, Horita Z, Matsuda K, Hirosawa S, Tsuji N. Mechanical properties and microstructure of 6061 aluminum alloy severely deformed by ARB process and subsequently aged at low temperatures. IOP Conference Series: Materials Science and Engineering. 2014;63:012088.
15. Dadbakhsh S, Karimi Taheri A, Smith CW. Strengthening study on 6082 Al alloy after combination of aging treatment and ECAP process. Materials Science and Engineering: A. 2010;527(18-19):4758-66.
16. Chou C-Y, Hsu C-W, Lee S-L, Wang K-W, Lin J-C. Effects of heat treatments on AA6061 aluminum alloy deformed by cross-channel extrusion. Journal of Materials Processing Technology. 2008;202(1-3):1-6.
17. Sivasankaran S, Sivaprasad K, Narayanasamy R, Iyer VK. Effect of strengthening mechanisms on cold workability and instantaneous strain hardening behavior during grain refinement of AA 6061-10wt.% TiO2 composite prepared by mechanical alloying. Journal of Alloys and Compounds. 2010;507(1):236-44.
18. Sahu P, De M, Kajiwara S. Microstructural characterization of stress-induced martensites evolved at low temperature in deformed powders of Fe–Mn–C alloys by the Rietveld method. Journal of Alloys and Compounds. 2002;346(1-2):158-69.
19. Alizadeh M, Paydar MH. High-strength nanostructured Al/B4C composite processed by cross-roll accumulative roll bonding. Materials Science and Engineering: A. 2012;538:14-9.
20. Alihosseini H, Asle Zaeem M, Dehghani K, Faraji G. Producing high strength aluminum alloy by combination of equal channel angular pressing and bake hardening. Materials Letters. 2015;140:196-9.
21. Fleischer RL. Solution hardening by tetragonal dist ortions: Application to irradiation hardening in F.C.C. crystals. Acta Metallurgica. 1962;10(9):835-42.
22. Fleischer RL. Substitutional solution hardening. Acta Metallurgica. 1963;11(3):203-9.
23. Amirkhanlou S, Ketabchi M, Parvin N, Orozco-Caballero A, Carreño F. Homogeneous and ultrafine-grained metal matrix nanocomposite achieved by accumulative press bonding as a novel severe plastic deformation process. Scripta Materialia. 2015;100:40-3.
24. Yoo SJ, Han SH, Kim WJ. Strength and strain hardening of aluminum matrix composites with randomly dispersed nanometer-length fragmented carbon nanotubes. Scripta Materialia. 2013;68(9):711-4.
25. Ma K, Wen H, Hu T, Topping TD, Isheim D, Seidman DN, et al. Mechanical behavior and strengthening mechanisms in ultrafine grain precipitation-strengthened aluminum alloy. Acta Materialia. 2014;62:141-55.
26. Rezaei MR, Shabestari SG, Razavi SH. Effect of ECAP consolidation temperature on the microstructure and mechanical properties of Al-Cu-Ti metallic glass reinforced aluminum matrix composite. Journal of Materials Science & Technology. 2017;33(9):1031-8.
27. Ye XX, Chen B, Shen JH, Umeda J, Kondoh K. Microstructure and strengthening mechanism of ultrastrong and ductile Ti-xSn alloy processed by powder metallurgy. Journal of Alloys and Compounds. 2017;709:381-93.
28. Humphreys FJ, Hatherly M. Recrystallization of Two-Phase Alloys. Recrystallization and Related Annealing Phenomena: Elsevier; 2004. p. 285-319.
29. Chen XH, Lu L, Lu K. Grain size dependence of tensile properties in ultrafine-grained Cu with nanoscale twins. Scripta Materialia. 2011;64(4):311-4.
30. Malopheyev S, Kulitskiy V, Kaibyshev R. Deformation structures and strengthening mechanisms in an AlMgScZr alloy. Journal of Alloys and Compounds. 2017;698:957-66.
31. Takata N, Ohtake Y, Kita K, Kitagawa K, Tsuji N. Increasing the ductility of ultrafine-grained copper alloy by introducing fine precipitates. Scripta Materialia. 2009;60(7):590-3.